

Navier-Stokes-driven analysis of mean and fluctuating wall shear stress in turbulent channel flow

Le Yin^{1†}, Yongyun Hwang² and John Christos Vassilicos^{1‡}

¹UMR 9014 - LMFL - Laboratoire de Mécanique des Fluides de Lille - Kampé de Fériet, Univ. Lille, CNRS, ONERA, Arts et Metiers Institute of Technology, Centrale Lille, F-59000 Lille, France

²Department of Aeronautics, Imperial College London, South Kensington, London SW7 2AZ, UK

(Received xx; revised xx; accepted xx)

We propose a Navier-Stokes-driven analysis of the mean and fluctuating wall shear stress (WSS) applied to turbulent channel flow data from direct numerical simulations at friction Reynolds numbers up to $Re_\tau \approx 2000$. Starting from the streamwise momentum equation, we derive exact integral equations that relate the square plane-average and the square fluctuating WSS to wall-normal integrals of terms combining shear with acceleration, shear with pressure-gradient, and shear with viscous diffusion. The square plane-average WSS can be well approximated by the product of plane-average shear and plane-average acceleration integrated over the buffer layer with corrections from the mean pressure gradient which diminish as the reciprocal of the Reynolds number. The square fluctuating WSS is similarly well approximated by the shear-acceleration and shear-pressure-gradient covariances integrated over the buffer layer, but the latter increases in magnitude with Reynolds number and is therefore not negligible. The acceleration fluctuations around the plane-average acceleration consist of a local Eulerian fluctuating acceleration, an advective acceleration and a term which gives rise a turbulence production contribution to the shear-acceleration covariance. By Taylor's frozen turbulence hypothesis the Eulerian acceleration and the streamwise mean advection part of the advective acceleration cancel each other. The shear-acceleration covariance is characterised by a near-wall peak which results from turbulence production and, more specifically, sweeps.

Key words: turbulent channel flow, boundary layer, turbulent theory

1. Introduction

Real world turbulent flows are often, if not always, bounded by walls. The flow may be considered external in the case of a turbulent boundary layers (TBL) or internal in the case of a turbulent channel flow (TCF) or turbulent pipe flow (TPF). The existence of a no-slip

† Email address for correspondence: le.yin@centralelille.fr

‡ Email address for correspondence: john-christos.vassilicos@cnrs.fr

boundary, together with fluid viscosity, gives rise to shear stresses close to the wall, which relaxe further away from the wall. Right at the wall, the stresses are naturally named wall shear stress. The surface integral of shear stresses at the wall in the streamwise direction constitutes a parallel force acting on the surface by the fluid, i.e. skin friction drag. The flow above the wall is often turbulent, and since turbulent flows are dynamic, i.e. fluctuating in space and time, the instantaneous and local-in-space wall shear stresses must also be fluctuating. The relationship between the wall shear stress and above fluid motion is best described by the Navier-Stokes equations. Understanding the dynamical process of wall shear stress necessitates studies of both the mean and the fluctuations around the mean, and is perhaps best undertaken through an analysis based on the Navier-Stokes equations.

1.1. Mean wall shear stress and skin friction identities

Many attempts have been made to relate the mean wall shear stress with physical processes above the wall by integrating the Navier-Stokes equations under certain assumptions. The employment of integration is a natural way to obtain relations of skin friction from the Navier-Stokes equations, since the skin friction comes out of the integrated wall-normal viscous diffusive term. von Kármán (1921) first integrated the streamwise boundary layer-approximated Navier-Stokes equation in the wall-normal direction from the wall to infinity and related the mean skin friction directly to displacement thickness and momentum thickness. Ligrani & Moffat (1986) adopted a similar strategy by integrating up to a finite distance from the wall. They obtained a momentum balance equation which was then used to experimentally estimate the skin friction from velocity and Reynolds shear stress measurement above the wall.

Integral relations have attracted more interest in the past two decades. Fukagata *et al.* (2002) derived a relation (FIK identity) by integrating the streamwise Reynolds-averaged Navier-Stokes equation three times in the wall normal direction. They obtained a relation (1.1) (in standard notation which, for economy of space, we do not define in this qualitatively descriptive introduction) which clearly distinguishes laminar and turbulent contributions to the mean skin friction coefficient C_f , plus an non-stationary non-homogeneous term,

$$C_f = \underbrace{\frac{12}{Re_b}}_{\text{Laminar}} + \underbrace{\int_0^\delta -(1-y)\langle u'v' \rangle dy}_{\text{weighted Reynolds stress}} - \underbrace{12 \int_0^\delta (1-y)^2 \left(I_x'' + \frac{\partial p''}{\partial x} + \frac{\partial \bar{u}}{\partial t} \right) dy}_{\text{Non-stationary non-homogeneous term}}. \quad (1.1)$$

Renard & Deck (2016) derived another relation (RD identity) of skin friction by integrating the mean energy equation once in the wall-normal direction in an absolute frame of reference moving with either the bulk flow velocity in internal flow, or the free stream velocity in external flow. While the RD identity (1.2) does not separate the laminar from the turbulent contributions as the effect of turbulence is implied in the mean shear profile which enters the mean dissipation, it describes the contributions to the skin friction through the mean dissipation and turbulent energy production plus the additional non-homogeneous term. In the case of TCF, the relation can be written as,

$$C_f = \underbrace{\frac{2}{U_b^3} \int_0^\delta \nu \left(\frac{\partial \langle u \rangle}{\partial y} \right)^2 dy}_{\text{Mean dissipation}} + \underbrace{\frac{2}{U_b^3} \int_0^\delta -\langle u'v' \rangle \frac{\partial \langle u \rangle}{\partial y} dy}_{\text{Turbulence production}} + \underbrace{\frac{2}{U_b^3} \int_0^\delta (\langle u \rangle - U_b) \frac{\partial}{\partial y} \left(\frac{\tau}{\rho} \right) dy}_{\text{Non-stationary non-homogeneous term}}. \quad (1.2)$$

Other such identities relating to skin friction are the doubly integrated boundary layer equation by Xia *et al.* (2015), the triply integrated mean vorticity equation by Yoon *et al.* (2016), the

integrated streamwise momentum equation with turbulent inertia replacing the Reynolds shear stress by (Zhao *et al.* 2024) and many others (Ricco & Skote 2022; Elnahhas & Johnson 2022, etc.).

Depending on the number of repeated integrations, there are an infinite number of integral identities relating the skin friction to different physical process above the wall (Ricco & Skote 2022; Elnahhas & Johnson 2022). With each identity, come correlations between physical processes, each with a different premultiplied weight. Nevertheless, the mean skin friction is merely the average over the weighted physical processes, and its value is independent of the formulation. Attempts to analyse the skin friction through averaging different physical processes inevitably leads to ambiguities due to differences in formulations. As an example, the study of Agostini & Leschziner (2019) used both FIK and RD identities to analyse the contribution of large-scale motions to the mean skin friction. Due to the different weights multiplying the Reynolds shear stress, the results from the two identities are quantitatively different in terms of percentage contribution to the mean skin friction by the large-scale motions.

What also remains unclear is whether the upper limit of the integration should be at infinity in external flows; at the axis or the plane of symmetry in internal flows; or at an arbitrary wall normal position. The former two choices, employed by von Kármán (1921); Fukagata *et al.* (2002); Xia *et al.* (2015); Renard & Deck (2016); Yoon *et al.* (2016); Elnahhas & Johnson (2022); Ricco & Skote (2022), rely on two potential reasons: (i) it is presumed that skin friction is influenced by the entire flow above the wall; (ii) it facilitates the treatment of certain terms that vanish away from the wall. However, choosing an arbitrary integration limit is also possible and sometime physically justified. In TBL, Ligrani & Moffat (1986) chose to integrate the boundary layer equation up to a finite height due to experimentally limited data very far from the wall. As it is not known *a priori* which physical processes far away from the wall contribute to the skin friction, Zhao *et al.* (2024) investigated how varying the upper limit of the integral terms in their identity affects contributions to the skin friction in TCF. Indeed, due to the aforementioned ambiguity in the formulation, different FIK-like identities may also display distinguishing behaviours in their variations with the upper limit of the integral, further obscuring the mean skin friction decomposition.

1.2. *Fluctuating wall shear stress*

The fluctuations of wall shear stress stem from the turbulent flow above the wall, as they are absent in a laminar steady flow. While most studies and practices in the turbulent regime concern the mean skin friction which contributes to the total mean drag, the fluctuations of wall shear stress also have wide implications, for example in cardiovascular disease (Zhou *et al.* 2023) and in structural fatigue modelling of wind turbine blades (Ravikumar *et al.* 2020).

The fluctuations of wall shear stress are known to be quite significant compared to its mean value. Schlatter & Örlü (2010) compiled fluctuating wall shear stress data from TCF, TPF and TBL and found that the root-mean-square (rms) of fluctuating wall shear stress normalised by the mean wall shear stress increases slowly with the logarithm of friction Reynolds number. At the highest Reynolds numbers available, the rms of wall shear stress can be more than 40% of the mean wall shear stress. Whether the rms of wall shear stress compared to its mean value is bounded or not remains an open fundamental question in wall-bounded turbulent flows. Assuming that the skin friction coefficient vanishes at infinite Reynolds number, the unboundedness of rms of wall shear stress compared to the mean wall shear stress would imply that for higher Reynolds number applications, such as large-scale wind turbines, one would have to consider the fluctuations of local stresses ever more carefully.

Additionally, the increase in the ratio of fluctuating wall shear stress to the mean wall

shear stress with increasing Reynolds number implies that universal scaling of second-order statistics does not hold close to the wall. This fact is also evident in the Reynolds number dependence of the near-wall peak of streamwise momentum variance.

The fluctuations of wall shear stress are not only characterised by their intense rms, but also by the nature of their higher order statistics. Direct numerical simulations (DNS) of turbulent boundary layers have shown that the wall shear stress follows an approximate log-normal distribution (Diaz-Daniel *et al.* 2017). This distribution features a heavy tail that favours the occurrence of large positive values of instantaneous local wall shear stress, becoming increasingly extreme with increasing Reynolds number. On the other side of the distribution, negative wall shear stresses or back flow events are also observed. This signifies the reversal of local streamwise velocity inside the viscous sublayer. These extreme backflow events have been shown to be associated with strong spanwise motions in the viscous sublayer (Diaz-Daniel *et al.* 2017).

Experimental measurement of instantaneous and local wall shear stress is a challenging task that requires forefront experimental techniques (Örlü & Vinuesa 2020). The behaviour of traditional sensors, such as hot-wires and hot-films, are significantly affected by the solid surface nearby, which introduces large thermal inertia and drifts the signals measured (Alfredsson *et al.* 1988). Moreover, it is impossible for these devices to keep track of backflow events due to their lack of response to flow direction. Only recently have advanced techniques, such as particle image velocimetry (PIV) and particle tracking velocimetry (PTV) within the viscous sublayer, enabled reliable identification of backflow events (Willert *et al.* 2018; Klinner & Willert 2025) in good agreement with DNS data.

To the authors' knowledge, there has been no attempt to date to describe the fluctuating wall shear stress using the Navier-Stokes equations to obtain an integral relation a bit like a FIK identity. Lee & Hwang (2025) analysed the fluctuating wall shear stress as turbulent dissipation at the wall by examining the streamwise turbulent kinetic energy budget close to the wall. They found that turbulent dissipation and transport spectra display universal behaviour for streamwise wavelength smaller than about 1000 viscous unit, and contribution for wavelength larger than 1000 viscous unit and smaller than half height/pipe radius increases with Reynolds number.

1.3. *Goal of the present work*

A natural attempt to study the wall shear stress and its fluctuations is by directly employing the streamwise momentum equation (streamwise component of the Navier-Stokes equations) to describe the wall shear stress. In the present work, we address the mean skin friction from an analysis of the plane-average streamwise momentum equation in TCF. From the the plane-average momentum balance, we derive a simple identity relating the square mean wall shear stress to the physical processes above the wall naturally imposed by the Navier-Stokes equations. An identity for the variance of the wall shear stress fluctuations is also derived along the same lines using the plane-fluctuating momentum balance. The physical processes above the wall which matter in this identity are also naturally imposed by the Navier-Stokes equations. The result shows that the fluctuating wall shear stress depends heavily on the fluctuating acceleration as well as the fluctuating pressure gradient, both becoming more intense with increasing Reynolds number. We study the extent from the wall that is required for these Navier-Stokes-derived processes to determine the mean wall shear stress and the variance of its fluctuations. We also identify and study the dominant processes and attempt to explain some of their features physically.

| Name | Re_τ | $N_x \times N_y \times N_z$ | Δx^+ | Δy^+ | Δz^+ | $T_{\text{int}} u_\tau / \delta$ | N_t |
|-------|-----------|------------------------------|--------------|--------------|--------------|----------------------------------|-------|
| R230 | 235 | $96 \times 193 \times 96$ | 11.52 | 0.53 – 4.53 | 5.76 | 183.20 | 3000 |
| R360 | 359 | $144 \times 257 \times 144$ | 11.74 | 0.61 – 5.19 | 5.87 | 172.24 | 3000 |
| R500 | 498 | $192 \times 289 \times 192$ | 12.22 | 0.75 – 6.41 | 6.11 | 164.46 | 3000 |
| R950 | 953 | $384 \times 513 \times 384$ | 11.69 | 0.80 – 6.91 | 5.85 | 151.55 | 3000 |
| R2000 | 2012 | $768 \times 1025 \times 768$ | 12.31 | 0.83 – 7.29 | 6.16 | 145.79 | 3151 |

Table 1: Numerical setup of DNS in FD TCF. N_x, N_y and N_z indicate the numbers of grid points in the streamwise, wall-normal and spanwise directions respectively; $\Delta x^+, \Delta y^+$ and Δz^+ indicate grid spacings, after de-aliasing, in inner units; T_{int} denotes the integration time after the initial transient and N_t denotes the number of instantaneous snapshots stored for post-processing.

2. DNS Data set

We use the data sets from direct numerical simulation (DNS) of incompressible FD TCF with constant mass flux at five different Reynolds numbers: $Re_\tau = 235, 359, 498, 953, 2012$, where Re_τ is the friction Reynolds number. The bulk velocity is kept constant by varying the instantaneous pressure gradient so that it remains equal to the sum of surface frictions on the two walls. The data sets are obtained with DNS performed using the Navier-Stokes solver `diablo` (Bewley 2014), employing the Fourier-Galerkin method with a 2/3 de-aliasing rule in the wall-parallel directions x and z , and a second-order finite difference method in the wall-normal direction y . The temporal discretisation of the solver is based on the fractional-step algorithm by Kim & Moin (1985), with implicit treatment of viscous terms using the Crank–Nicolson scheme and explicit treatment of the remaining terms using a low-storage third-order Runge–Kutta scheme. It is the same data set used by Yin *et al.* (2024), except that the R2000 simulation has been continued up to $T_{\text{int}} u_\tau / \delta = 145.79$ for better convergence of statistics (see exact definition of u_τ in sub-section 3.1). We denote the streamwise, wall-normal, and spanwise directions by (x, y, z) , with the corresponding velocity field components $(u, v, w) \equiv (u_1, u_2, u_3)$. The size of the simulation domain is set to be $L_x = \pi\delta$, $L_y = 2\delta$, and $L_z = \pi\delta/2$, where δ is the half channel height. The spanwise extent of the simulation box is comparable to the minimal unit for the self-sustaining process of the largest energy-containing structures as per Hwang & Cossu (2010) and Hwang & Bengana (2016). Adhering to previous studies, the size of the computational domain is deliberately chosen to be small in order to capture single entities of the large-scale energy-containing structures without significantly modifying the mean statistics (Lozano-Durán & Jiménez 2014). Details of the DNS data set and its naming convention can be found in table 1.

3. Plane-average wall shear stress

As pointed out in §1, we aim to study the wall shear stress using the Navier-Stokes equations. The wall shear stress is a consequence of fluid motion above the wall, the adherence of fluid at the wall, and the effect of viscous momentum diffusion in the vicinity of the wall. It is therefore natural to extract the wall shear stress directly from the diffusive term of the Navier-Stokes equations. The only way that the Navier-Stokes equations can be recast so as to give formulae for fluctuating wall shear stress moments in terms of fluid flow quantities above the wall is by multiplying the fluctuating momentum equation by a power of the kinematic viscosity times the fluctuating streamwise velocity gradient in the wall normal direction, and then integrating in the wall-normal direction from the wall to some distance from the wall. Depending on the order of the term multiplying the Navier-Stokes equations (the value of the aforementioned power), one obtains an equation that exactly describes any order statistics

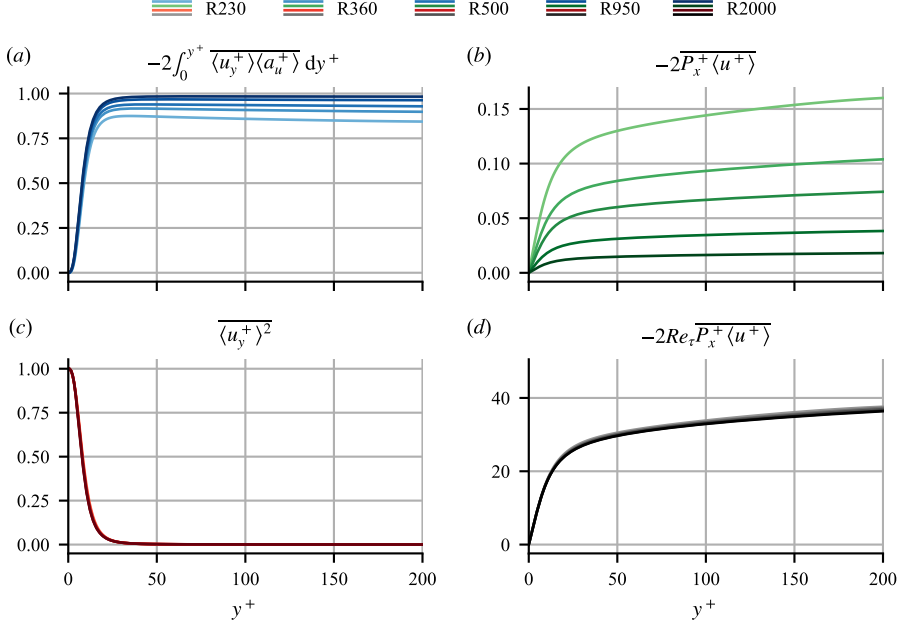


Figure 1: Contribution to the square plane-average wall shear stress in equation (3.2).

of the fluctuating wall shear stress as explained in Appendix A. In this work, we apply this procedure to the variance of the fluctuating wall shear stress but start by studying the mean wall shear stress. We apply a similar procedure to obtain a closed form equation for the square of the mean wall shear-stress as explained in the following subsection. The present study is therefore limited to the mean wall shear stress and the variance of wall shear stress, i.e. the first and second order statistics.

3.1. Derivation of plane-average mean equation

We consider the plane-averaged streamwise Navier-Stokes equation:

$$\langle a_u \rangle = -P_x + \nu \langle u_{yy} \rangle, \quad (3.1)$$

where a_u is the fluid particle acceleration comprised of Eulerian acceleration plus non-linear advection, P_x is the (x, z) plane-averaged pressure gradient (implicitly normalised by mass density), u_{yy} stands for $\frac{\partial^2}{\partial y^2} u$, ν is the kinematic viscosity, and the brackets represent averaging in a wall-parallel plane, i.e. $\langle A \rangle = \frac{1}{L_x L_z} \iint A \, dx \, dz$. (The wall-parallel diffusion term averages to zero due to periodicity in the wall-parallel boundary conditions.) We now multiply both sides of equation (3.1) at arbitrary y by $\nu \langle u_y \rangle(y) = \nu \frac{\partial}{\partial y} \langle u \rangle(y)$ at a given y , and integrate the equation in the y direction from $y = 0$ at the wall to some arbitrary y :

$$\begin{aligned} \nu \int_0^y \langle u_y \rangle \langle a_u \rangle \, dy' &= -\nu \int_0^y \langle u_y \rangle P_x \, dy' + \frac{1}{2} \left[\nu^2 \langle u_y \rangle^2(y, t) - \nu^2 \langle u_y \rangle^2(y = 0) \right] \\ \Rightarrow \langle \tau_w \rangle^2(t) &= -2\nu \int_0^y \langle u_y \rangle \langle a_u \rangle \, dy' - 2\nu P_x \langle u \rangle(y, t) + \nu^2 \langle u_y \rangle^2(y, t). \end{aligned} \quad (3.2)$$

We obtain this exact formula (3.2) for the time-fluctuating plane-averaged wall shear stress as a sum of three different quantities that depend on y distance from the wall. As the left-

hand-side of the equation (3.2) is independent of y , the y -dependencies of the right hand side terms cancel at every y . When taking $y = 0$ on the right hand side, this relation reduces to the definition of the local wall shear stress, i.e. $\tau_w(x, z, t) \equiv \nu u_y(x, y = 0, z, t)$, with vanishing shear-acceleration term and pressure-velocity term.

Defining the time average $\bar{A} = \lim_{T \rightarrow \infty} \frac{1}{T} \int_0^T A(t) dt$ for any variable $A(t)$, the time-averaged terms on the right hand side of equation (3.2) are plotted in figure 1(a, b, c). When presented with superscript $(\cdot)^+$, the results are normalised by the usual inner units, i.e. the friction velocity u_τ defined from the space-time average wall shear stress $u_\tau^2 = \overline{\langle \tau_w \rangle}$, and the viscous wall unit $\delta_\nu = \nu/u_\tau$. From (3.2), the sum of the three quantities plotted in figure 1(a, b, c) equals $\overline{\langle \tau_w \rangle}^2/u_\tau^2$ which is very close to 1 (see following paragraph).

Due to the minimal computational domain, the plane-average wall shear stress $\langle \tau_w \rangle(t)$ fluctuates in time. Its time fluctuation in terms of rms is less than 5% of its time average value for all five Reynolds numbers. The time-average squared wall shear stress therefore contains less than 0.25% deviation, which is insignificant compared to the square of the time-average wall shear stress. Numerical integration in the wall-normal direction is performed with cubic spline, and the resulting numerical error is within 1% of the square mean WSS.

3.2. Estimate of wall shear stress and Reynolds number dependencies

The time-average square mean shear stress $\overline{\langle u_y^+ \rangle^2}$ normalised by inner units shown in figure 1(c) is near-equal to 1 at the wall and reduces monotonically as y increases further away from the wall. At $y^+ \approx 54$, $\overline{\langle u_y^+ \rangle^2}$ drops below 0.2% of time-average square wall shear stress $\overline{\langle \tau_w \rangle^2}/u_\tau^4$ for all five Reynolds numbers. Similar to the δ_{99} definition for the turbulent boundary layer thickness, we may define a position $\delta_w = \delta_{0.2\%} \equiv 54\delta_\nu$ as a cut-off wall normal position. Changing the cut-off threshold, the 1% cut-off position is around $31\delta_\nu$ for example. This cut-off position identifies the y -location above which only the shear-acceleration term plotted in figure 1(a) and the pressure-velocity term plotted in figure 1(b) effectively (if not overwhelmingly) contribute to $\overline{\langle \tau_w \rangle^2}$. (Note that the local contribution from the molecular shear stress vanishes beyond this cut-off position, as plotted in figure 1(c).) The dominance of these two contributions to $\overline{\langle \tau_w \rangle^2}$ is confirmed by figure 2(a) where we plot the percentage contribution to $\overline{\langle \tau_w \rangle^2}$ from these two terms as a function of the upper y limit of the integral. It is found that the corresponding curves for the five Reynolds numbers collapse rather well, but not perfectly. This result suggests that the buffer layer encodes within it all the necessary information required to calculate the plane-average WSS.

To better appreciate this result, it may help to spell out the differences between equation (3.2) and the usual integrated mean momentum equation obtained by directly integrating (3.1) over y :

$$\langle \tau_w \rangle = - \int_0^y \langle a_u \rangle dy' - P_x y + \nu \langle u_y \rangle(y, t). \quad (3.3)$$

The integrand $\langle u_y \rangle \langle a_u \rangle$ in the first term of the right hand side of (3.2) decays to zero with increasing y' whereas the integrand $\langle a_u \rangle$ in the first term of the right hand side of (3.3) does not. In particular, time averaging of both sides of (3.3) leads to $\overline{\langle \tau_w \rangle} = -\overline{\langle uv \rangle}(y) - \overline{P_x} y + \nu \overline{\langle u_y \rangle}(y)$ which makes it clear that $\int_0^y \overline{\langle a_u \rangle} dy' = \overline{\langle uv \rangle}(y)$ does not tend to become independent of y with increasing y as it would if $\overline{\langle a_u \rangle}$ decayed to 0 fast enough with increasing y' . Hence whilst the first term on the right hand side of (3.2) does not grow with y above δ_w , the first term on the right hand side of (3.3) does, and this is particularly clear from the time averaged form of equation (3.3) where $-\overline{\langle uv \rangle}(y)$ continues growing till y reaches

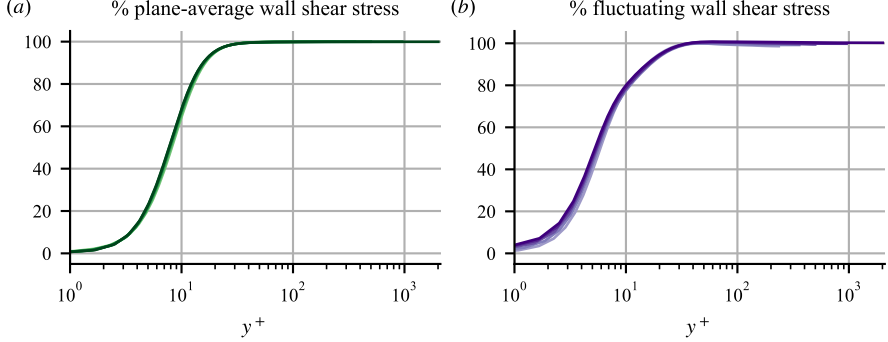


Figure 2: Percentage contribution from shear-acceleration plus shear-pressure-gradient to (a) plane-average and (b) fluctuating wall shear stresses. Results from five Reynolds numbers collapse rather well.

$y_m \sim \sqrt{\delta_v \delta}$. Indeed, the wall distance $y_m \sim \sqrt{\delta_v \delta}$ where $-\overline{\langle uv \rangle}$ is maximal follows directly by assuming a log law for $\langle u \rangle$ (see e.g. Afzal 1984; Panton 2007; Lee & Moser 2015; Hwang & Lee 2020). This length scale $\sqrt{\delta_v \delta}$ characterises the mesolayer (Afzal 1984) and is larger than δ_w which scales with δ_v . Note that the linear dependence on y of the pressure term on the right hand side of (3.3) is essential for obtaining this mesolayer length scale and that the dependence on y of the pressure term on the right hand side of (3.2) is much weaker than linear. Given these important differences between the integrated momentum equation (3.3) and our equation (3.2), it is not possible to use the integrated mean momentum equation (3.3) to encode within the buffer layer all necessary information required to calculate the plane-average WSS as it is with our equation (3.2).

We now focus on the terms on the right hand side of equation (3.2). While $\overline{\langle u_y^+ \rangle^2}$ shows little Reynolds number dependence close to the wall (figure 1c), both the shear-acceleration and the pressure-velocity terms show significant Reynolds number effects (figure 1a, b). The latter's Reynolds number dependence can be estimated as follows. In a constant mass flux channel, the plane-average pressure gradient balances the sum of the plane integrals of wall shear stresses on the two walls instantaneously. By assuming that the plane-average pressure gradient does not correlate heavily in time with the plane-average velocity profile, one can estimate the mean pressure gradient as the squared friction velocity divided by the channel half height, i.e.

$$-\nu \overline{P_x \langle u \rangle} / u_\tau^4 \approx \frac{\nu \overline{\langle u \rangle} u_\tau^2}{u_\tau^4 \delta} = \frac{\overline{\langle u \rangle}}{u_\tau} \frac{\nu}{\delta u_\tau} = \frac{U^+(y^+)}{Re_\tau}, \quad (3.4)$$

where $U^+(y^+)$ is the mean velocity profile scaled in inner units which may be assumed to be invariant with Reynolds number in the near-wall region. We therefore plot in figure 1(d) the pressure velocity term multiplied by Re_τ . The product collapses approximately for all five Reynolds numbers. The slight mismatch between the proposed scaling and the data from the current simulation may be due to two main possible causes: time correlations between the time fluctuations of the plane-average pressure gradient and the plane-average velocity; and residual weak Reynolds number effects on the mean velocity profile. We note that the above balance would be exact in a constant pressure gradient channel (with \approx replaced by $=$).

At high enough Reynolds number, we therefore have the following estimation of the time-average square mean wall shear stress in terms of the product between the mean shear and the plane-average acceleration integrated from the wall to some finite distance from the wall, plus a correcting pressure-velocity term that is proportional to $1/Re_\tau$ (this estimate is acceptable

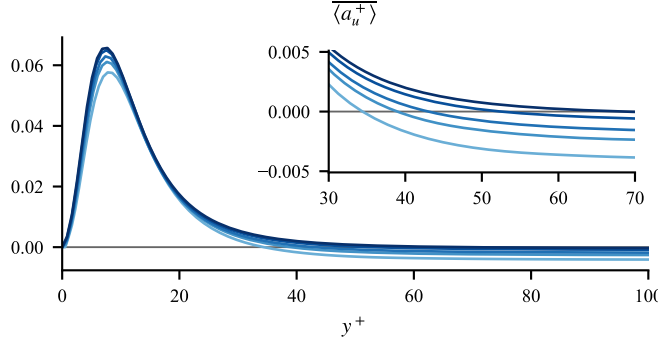


Figure 3: Mean acceleration profile.

even without time-averaging):

$$\overline{\langle \tau_w \rangle^2} \approx -2\nu \int_0^{\delta_w} \overline{\langle u_y \rangle \langle a_u \rangle} dy' + O(1/Re_\tau). \quad (3.5)$$

This result signifies the existence of a cut-off wall-normal distance $y = \delta_w$ which seems to scale with δ_ν , and beyond which there is no more additive contribution from the shear-acceleration term to $\overline{\langle \tau_w \rangle^2}$. The pressure gradient contribution vanishes at a $1/Re_\tau$ rate at large Reynolds numbers. We note that such interpretation is limited to the derived identity, and does not necessarily apply to other identities, for reasons explained in §1.1. Once sufficient information regarding the plane-average acceleration and shear near the wall (viscous and buffer layers) are gathered, it is possible to estimate $\overline{\langle \tau_w \rangle^2}$ exclusively based on near-wall data. Note, however, that δ_w/δ_ν may have a weak dependence on Re_τ which cannot be captured with the range of Reynolds numbers of our DNS data sets and which may imply that information regarding the plane-average acceleration and shear may also be required from above the buffer layer at some enormous value of Re_τ .

As all indications to date are that the mean skin friction coefficient has a weak dependence on Re_τ with increasing Re_τ , one may also expect $\overline{\langle \tau_w \rangle^2}$ to have such an asymptotic dependence. This dependence may come either from a Re_τ dependence of δ_w/δ_ν which is beyond our reach in this paper, or from the Re_τ dependence of the integrand in the integral on the right hand side of (3.5), or both. The plane-average shear profile $\overline{\langle u_y \rangle}$ may be considered as almost fully scaling in inner units near the wall. (This is reminiscent of the law of the wall, which states that the time- and plane-average shear profile $\overline{\langle u_y \rangle}$ fully scales in inner units near the wall.) However, the plane-average acceleration $\overline{\langle a_u \rangle}$ (figure 3) is composed of the plane-average Eulerian acceleration and the Reynolds shear stress gradient, the latter clearly depending on Reynolds number. Even in the minimal computational domain, the plane-average Eulerian acceleration is less than 1% of the plane-average Reynolds shear stress gradient. The gradient of Reynolds shear stress is known to cross zero (local maximum of Reynolds shear stress) at a y^+ that increases with Reynolds number. Reynolds number dependencies in magnitude and in zero-crossing location are clearly shown in figure 3 where we plot the wall-normal profile of $\overline{\langle a_u \rangle}$ in inner coordinates. If δ_w/δ_ν is independent of Re_τ then all the information required to calculate $\overline{\langle \tau_w \rangle^2}$ from the fluid flow can be found between the wall and the outer edge of the buffer layer for any Reynolds number. However, this thin near-wall region will then need to be Reynolds number dependent if $\overline{\langle \tau_w \rangle^2}$ is Reynolds

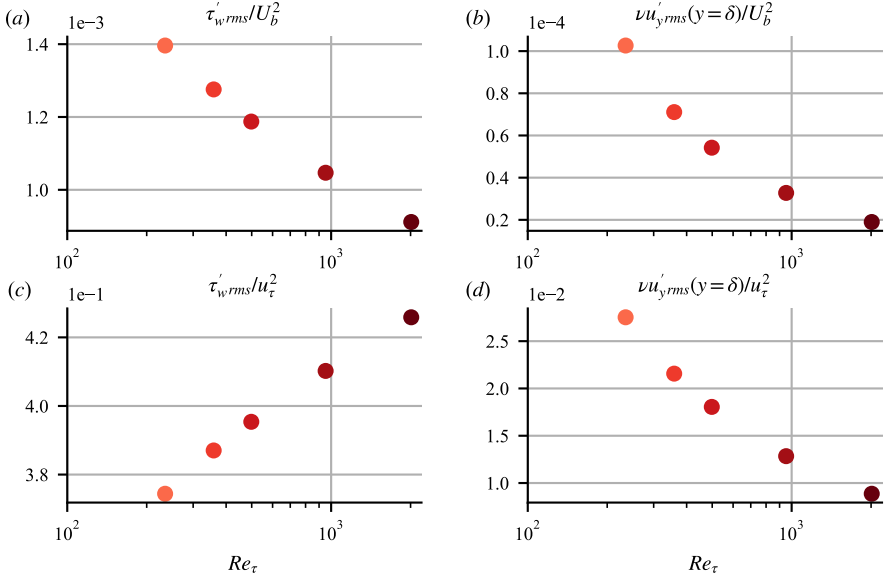


Figure 4: rms of fluctuating wall shear stress and local shear at channel centre normalised by bulk quantities (a, b) and by inner quantities (c, d)

number dependent, and this Reynolds number dependence will reflect a dependence of this thin near-wall region on the outer flow.

4. Wall shear stress fluctuations

Our method for analysing local quantities at the wall relies on the integration of the wall-normal diffusion term appearing in the Navier-Stokes equations, whether it is plane-averaged or plane-fluctuating. Our analysis of the fluctuating wall shear stress directly from the Navier-Stokes equations leads to a relation in terms of covariances that is neither an energy nor a momentum balance. Without any assumptions, this relation includes the covariances that are most direct and natural from the Navier-Stokes equations for the mean and fluctuations of square wall shear stress.

A lesson learnt from the analysis of cut-off height in the previous section is that nearly all the information needed to determine the mean wall shear stress can be found in the viscous and buffer layers at the Reynolds numbers of the present DNS data. The question naturally arises whether such cut-off wall-normal height also exists for the fluctuating wall shear stress.

To derive a formula for the variance of fluctuating wall shear stress from the Navier-Stokes equations, we first multiply the fluctuating wall-normal diffusion term in that equation with the fluctuating shear stress at the same y , average in x - z plane, and then integrate in the y direction from the wall to an arbitrary y :

$$\nu^2 \int_0^y \langle u'_y u'_{yy} \rangle dy' = \frac{\nu^2}{2} \int_0^y \frac{\partial}{\partial y} \langle u'_y u'_y \rangle dy' = \frac{\nu^2 \langle u'_y^2 \rangle(y, t)}{2} - \frac{\langle \tau'_w^2 \rangle(t)}{2}, \quad (4.1)$$

where the prime symbol denotes the plane-fluctuating part of a quantity, i.e.: $A'(x, y, z, t) = A(x, y, z, t) - \langle A \rangle(y, t)$. We see how this operation leads to the appearance of the variance of fluctuating wall shear stress $\langle \tau'_w^2 \rangle(t)$ so that when applied to all the terms of the Navier-Stokes equations at the start of sub-section 4.1, this operation yields a formula for $\langle \tau'_w^2 \rangle(t)$

in terms of fluid flow statistics above the wall. However, an additional interesting feature of equation (4.1) is the appearance of the variance of the local shear stress which is not zero at the channel centre, in contrast to the mean shear which is zero at the channel centre due to symmetry. Before proceeding with the Navier-Stokes equations in the following sub-section, we compare the Reynolds number dependencies of the two variances on the right hand side of equation (4.1) for $y = \delta$.

If normalised by δ/U_b , the time-average rms of the fluctuating shear $u'_{y rms}(y) \equiv \sqrt{\langle u'_y^2 \rangle}(y)$ increases with increasing Re_τ both at $y = 0$ and $y = \delta$. However these increases are slower than $1/\sqrt{y}$ because $\tau'_{w rms} \equiv vu'_{y rms}(y = 0)$ and $vu'_{y rms}(y = \delta)$ both decrease with increasing Re_τ when normalised by U_b^2 as shown in figure 4(a,b) for the five Reynolds numbers available. It is noticeable that $vu'_{y rms}(y = \delta)/U_b^2$ decreases much faster with increasing Re_τ than $\tau'_{w rms}/U_b^2$. This difference appears more dramatically when normalising by u_τ^2 . Figure 4(c) shows that $\tau'_{w rms}/u_\tau^2$ increases with increasing Re_τ , confirming the observation in Schlatter & Örlü (2010), whereas figure 4(d) shows that $vu'_{y rms}(y = \delta)/u_\tau^2$ decreases with increasing Re_τ . Similarly to our treatment of the mean wall shear stress, this observation could contribute to the existence of a cut-off height for the fluctuating wall shear stress equation, an issue which we address in the following sub-section.

4.1. Formula for the wall shear stress variance and time-average statistics

We consider the plane-fluctuating streamwise momentum equation:

$$a'_u = -p'_x + \nu \nabla^2 u'. \quad (4.2)$$

We first multiply the above equation by vu'_y , average over the x - z plane, integrate in the wall-normal direction from the wall to some arbitrary y and using equation (4.1) we obtain

$$\langle \tau_w'^2 \rangle = -2\nu \int_0^y \langle u'_y a'_u \rangle dy' - 2\nu \int_0^y \langle u'_y p'_x \rangle dy' + 2\nu^2 \int_0^y \langle u'_y u'_{//} \rangle dy' + \nu^2 \langle u'_y^2 \rangle, \quad (4.3)$$

where p'_x is the fluctuating streamwise pressure gradient (implicitly normalised by the mass density), $u'_{//} = u'_{xx} + u'_{zz}$ is the sum of the second derivatives in x and z directions of the streamwise velocity, and $\tau'_w \equiv vu'_y(y = 0)$ is the fluctuating wall shear stress that appears from the vertical momentum diffusion term. To the authors' knowledge, this is the first exact relation describing the spatially fluctuating wall shear stress directly using the Navier-Stokes equations.

The wall-normal profile of each time averaged budget term on the right hand side of equation (4.3) is plotted in figure 5 normalised in inner units. The major contribution to the wall shear stress fluctuations far enough from the wall is the positive contribution from the integrated shear-acceleration covariance attenuated by the negative contribution from the integrated shear-pressure-gradient covariance at normalised wall distances y^+ below 100. The latter contribution turns from negative to positive around $y^+ \approx 100$ but remains relatively minor at $y^+ > 100$. The two terms on the right hand side of equation (4.3) stemming from viscous diffusion diminish in magnitude with wall distance and appear to quickly become negligible as shown in figure 5(c, d). Whilst the profiles of these two viscous diffusion-related terms collapse rather well in inner units (except very near the wall for $\nu^2 \langle u'_y^2 \rangle$) the two main contributions to $\langle \tau_w'^2 \rangle$ display a significant increase in magnitude with increasing Re_τ in figure 5(a, b) where they are plotted in inner units. The magnitude of the negative integrated shear-pressure-gradient covariance increases around $y^+ \approx 20$ with increasing Reynolds number, as

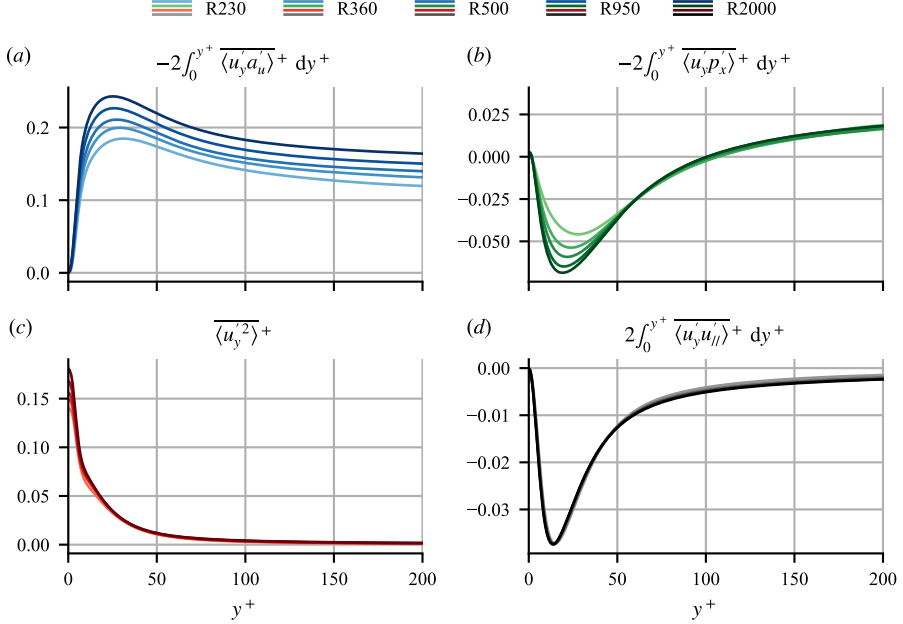


Figure 5: Contributions to the square plane-fluctuating wall shear stress in equation (4.3).

opposed to the diminishing contribution of the plane-average pressure-velocity term to the mean wall shear stress.

The major contribution to both the plane-average and the fluctuating wall shear stress comes from an integral involving shear and acceleration, with some correction from the term involving pressure. We plot in figure 2(b) the time-integrated sum of the y -integrated shear-acceleration covariance and the y -integrated shear-pressure-gradient covariance as a percentage contribution to $\langle \tau_w'^2 \rangle$. The percentage is given as a function of the upper y limit of the integrals. Even though there is no plateau reaching behaviour in figure 5(a, b) as there is in figure 1(a) so that both the shear-acceleration and the shear-pressure-gradient terms contribute significantly to the fluctuating wall shear even beyond $y^+ > 200$, the percentage plotted in figure 2(b) does reach a plateau beyond $y^+ \approx 30$. This observation stems from the approximate balance between fluctuating acceleration and fluctuating pressure far from the wall where fluctuating viscous diffusion is negligible (see §§4.2). As a result, we may expect the following estimate for the variance of the fluctuating wall shear stress:

$$\overline{\langle \tau_w'^2 \rangle} \approx -2\nu \int_0^{\delta_{w'}} \overline{\langle u'_y a'_u \rangle} dy' - 2\nu \int_0^{\delta_{w'}} \overline{\langle u'_y p'_x \rangle} dy'. \quad (4.4)$$

This estimate parallels the estimate (3.5) for the mean wall shear stress. For the Reynolds numbers accessible by our FD TCF data, the Navier-Stokes equations implies that one can predict the wall shear stress mean and variance from statistics involving mean/fluctuating shear, acceleration and pressure gradient between the wall and the upper edge of the buffer region. Similar to the estimate (3.5), the choice of the upper limit $\delta_{w'}$ of the integral in y depends on the threshold we chose for deciding that the percentage in figure 2(b) is close enough to 100%. Comparing figures 2(a) and 2(b), the percentage contribution to the fluctuating wall shear stress shows slightly larger variability with varying Reynolds numbers. This observation suggests that $\delta_{w'}$ in equation (4.4) may have a slightly stronger dependence

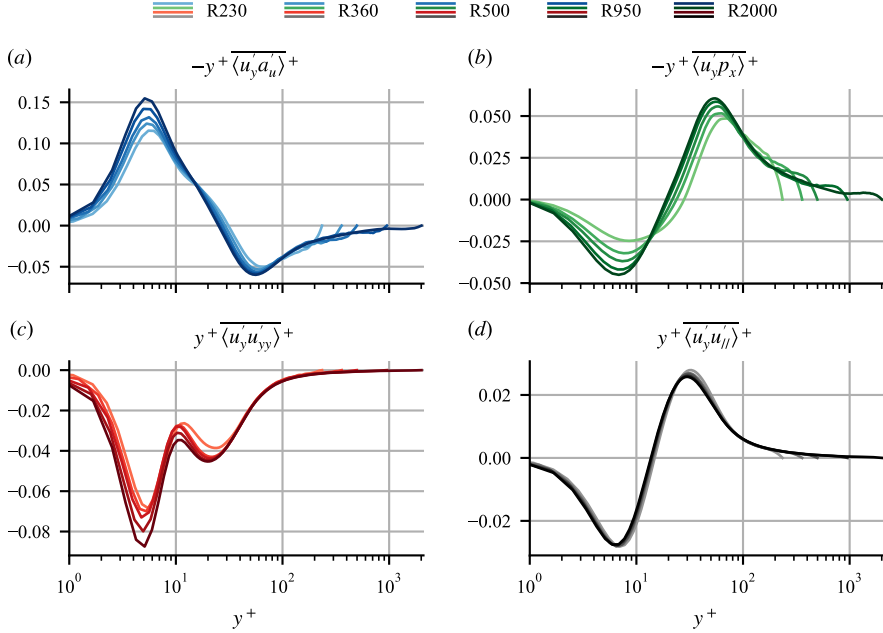


Figure 6: Premultiplied integrand contribution to square fluctuating plane-average wall shear stress.

on Re_τ than δ_w in equation (3.5). However, the Reynolds number dependence of $\overline{\langle \tau'_w \rangle^2}$ shown in figure 4(a, c) may also arise from the integrands inside the integrals in equation (4.4). Even so, equation (4.4) suggests that the variance of the fluctuating WSS is fully encoded within the buffer layer, i.e. that it is possible to obtain it from information within it.

In figure 6(a) and (b) we plot these two integrands in inner units as functions of y^+ . As the vertical axis is linear and the horizontal axis is logarithmic, we premultiply them by y^+ to ensure that the integral over $\log y^+$ is the same. Plotted in the same way in figure 6(c) is the spatial covariance between local shear and wall-parallel diffusion of streamwise fluctuating velocity, whose integral gives the difference between fluctuating wall shear stress and local-in- y streamwise shear (see relation 4.1). The sum of the four covariances in figure 6(a, b, c, d) is zero at each y^+ , as they are exactly balanced by the streamwise momentum equation. It is not until the channel centre $y^+ = Re_\tau$, the plane of symmetry, that the differential contribution from the shear-acceleration covariance becomes zero. The premultiplied shear-acceleration covariance (figure 5a) and shear-pressure-gradient covariance (figure 5b) beyond $y^+ = 30$ seem to cancel each other far enough from the wall, sharing similar positive/negative peak location around $y^+ \in [50, 60]$ as well as peak magnitudes. This observation is consistent with the integral estimate (4.4) and the integral profiles plotted in figure 5. Concerning Reynolds number dependence, a discussion that parallels the discussion at the end of §§3.2 could be repeated here for $\overline{\langle \tau'_w \rangle^2}$ and referring to figure 5(a, b) rather than $\overline{\langle \tau_w \rangle^2}$ and referring to figure 3.

4.2. Pressure and acceleration

The fluctuating acceleration, pressure gradient and viscous diffusion are related exactly by the fluctuating streamwise momentum equation (4.2). Approaching the wall as $y^+ \rightarrow 0$, velocity and acceleration vanish, resulting in the balance $p'_x \approx vu'_{yy}$ in some typical sense sufficiently

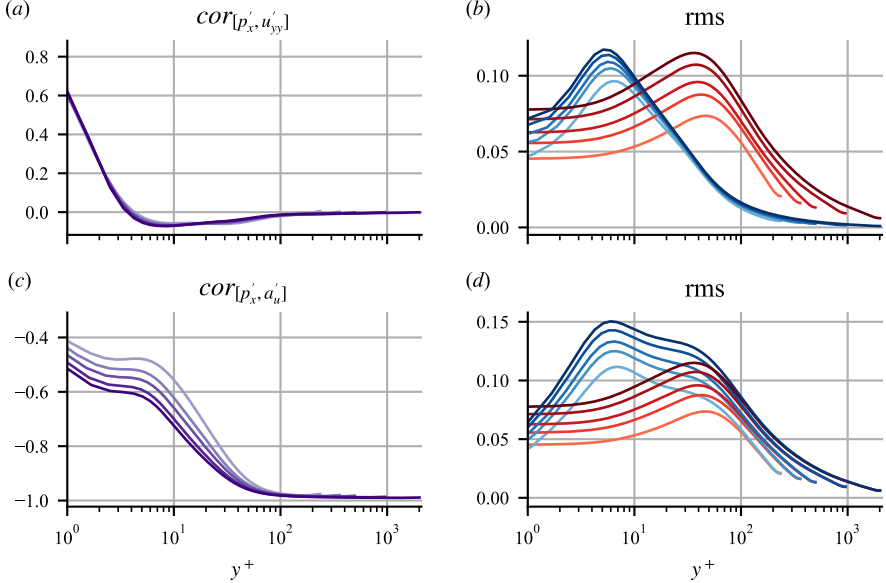


Figure 7: Pressure effect. (a) and (c): correlation of streamwise pressure gradient, vertical viscous diffusion and acceleration. In (b) and (d), red: rms of pressure gradient fluctuation. In (b) blue, rms of vertical viscous diffusion. In (d) blue, rms of streamwise acceleration. All rms are normalised in inner units.

close to the wall. Further away from the wall, i.e where $y^+ \gg 1$, the viscous diffusion as the solenoidal part of the force (normalised by mass density) balancing the acceleration, becomes less and less dominant. We expect therefore $a'_u \approx -p'_x$ to typically hold away from the wall, thereby explaining the self-cancelling behaviour in figure 6(a, b). To examine the validity of these two approximations, we plot in figure 7(a) and 7(c) the correlation coefficient between pressure gradient and vertical viscous diffusion of streamwise momentum, and the correlation coefficient between pressure gradient and streamwise acceleration respectively. For zero-mean variables $A(x, y, z, t)$ and $B(x, y, z, t)$ fluctuating in space and time, we define a spatial correlation coefficient as:

$$cor[A, B](y) = \overline{\left(\frac{\langle AB \rangle}{\sqrt{\langle A^2 \rangle} \sqrt{\langle B^2 \rangle}} \right)}. \quad (4.5)$$

Inside the viscous sublayer and above the wall, the correlation coefficient between pressure gradient and vertical diffusion (figure 7a) reduces quickly with distance from the wall. The correlation coefficient between pressure gradient and acceleration (figure 7c) remains negative inside the viscous sublayer, showing very significant anti-correlation. These two observations combined indicate that, inside the viscous sublayer $y^+ < 10$, both viscous diffusion and pressure gradient contribute to the acceleration, and the three quantities are comparable to each other in their rms (figure 7b, d) and correlations. The respective rms values shown are consistent with the study of Yeo *et al.* (2010) (see their figures 3 and 4). Significant deviations to the pressure-diffusion balance, which is actually exact at the wall, already occur extremely close to the wall as acceleration quickly develops.

In the range of $10 < y^+ < 100$, the rms of vertical diffusion quickly reduces and the correlation between streamwise pressure gradient and acceleration quickly develops, attaining nearly -1 as an almost perfect anti-

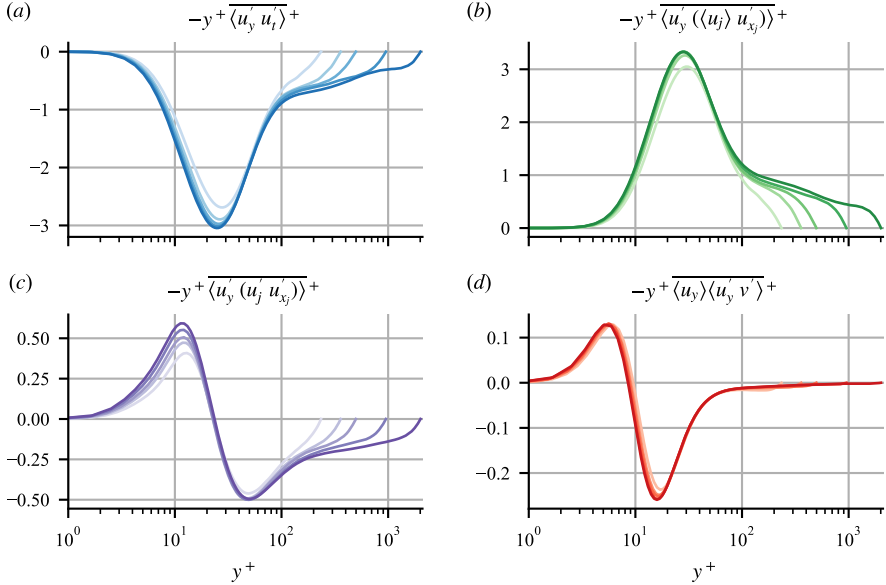


Figure 8: Decomposed acceleration contributions.

correlation can be found in isotropic turbulence even at moderate Reynolds number (e.g. see figure 4 in Tsinober *et al.* (2001)). Above $y^+ > 100$, the rms values of pressure and acceleration almost coincide. The self-cancellation between pressure gradient and acceleration is therefore supported by the almost perfect anti-correlation and coinciding rms values, and also evidenced by the absence of viscous diffusion far from the wall.

4.3. Taylor's hypothesis

Among the four premultiplied covariances presented in figure 6, the shear-acceleration covariance provides the largest contribution to $\langle \tau_w^2 \rangle$. We investigate this primary contribution to the wall shear stress fluctuation variance by applying the Reynolds decomposition and decomposing acceleration into five parts:

$$a'_u = u'_t + \langle u_j \rangle u'_{x_j} + u'_j u'_{x_j} + u'_j \langle u_{x_j} \rangle - \langle u'_j u'_{x_j} \rangle, \quad (4.6)$$

where $u'_t = \frac{\partial}{\partial t} u'$ is the plane-fluctuating local acceleration in the Eulerian frame of reference, i.e. fixed with respect to the wall; $\langle u_j \rangle u'_{x_j} = \langle u \rangle u'_x + \langle w \rangle u'_z$ (u'_x and u'_z stand for $\frac{\partial}{\partial x} u'$ and $\frac{\partial}{\partial z} u'$ respectively) is the advection of the fluctuating velocity field by the mean field, with the mean wall-normal velocity $\langle v \rangle$ being zero in TCF (plane-averaging the continuity equation and integrating in the wall-normal direction from the wall leads to $\langle v \rangle = 0$); $u'_j u'_{x_j}$ (with Einstein summation over $j = 1, 2, 3$ and u'_{x_j} standing for $\frac{\partial}{\partial x_j} u'$) is the self-advection of fluctuating velocity field; $u'_j \langle u_{x_j} \rangle = v' \langle u_y \rangle$ (u_{x_j} stands for $\frac{\partial}{\partial x_j} u$) is a term related to turbulent kinetic energy production, as it involves the interaction between the fluctuating velocity field and the mean shear; and finally $\langle u'_j u'_{x_j} \rangle$ is the plane-average Reynolds shear stress gradient, who does not correlate with fluctuating shear and therefore has no contribution in the fluctuating wall shear stress. The premultiplied covariances between the fluctuating streamwise shear and each one of the four fluctuating components making up a'_u in equation (4.6) are shown

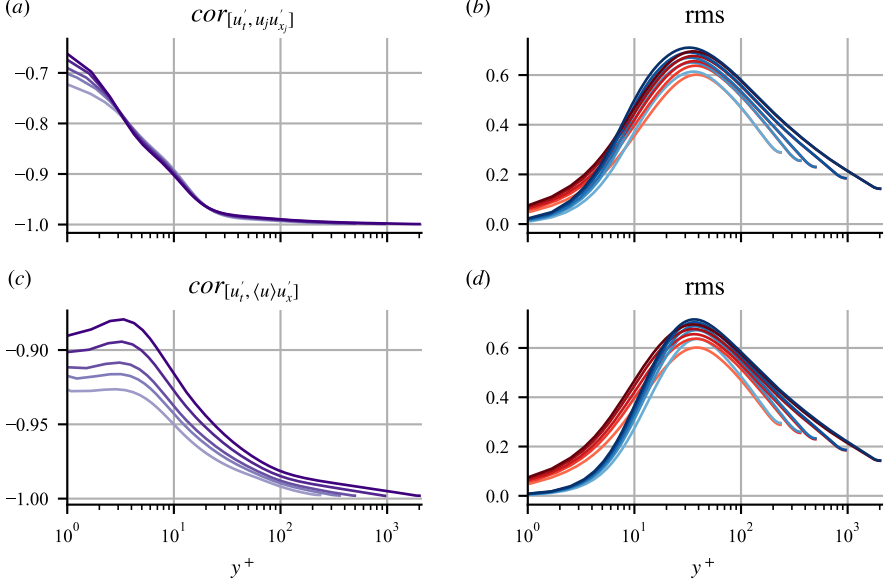


Figure 9: Taylor's hypothesis tested with correlation coefficient and rms values. (a) and (c): correlation of Eulerian acceleration and streamwise advection. In (b) and (d), red: rms of fluctuating Eulerian acceleration. In (b) blue, rms of advection of fluctuating velocity by total velocity. In (d) blue, rms of mean advection of fluctuating velocity. All rms are normalised in inner units.

in figure 8. The sum of these four covariances is equal to the fluctuating shear-acceleration covariance in figure 6(a).

Upon first observation, we notice that the magnitude of the covariance of local shear with Eulerian acceleration (figure 8a) and that with mean advection (figure 8b) are opposite in sign and at least one order of magnitude larger than the overall covariance between shear and Lagrangian acceleration in figure 6(a), as if they almost cancel each other. It is therefore sensible to investigate whether and to what extent the local Eulerian acceleration of the fluctuating streamwise velocity is mainly due to local mean advection of that velocity, i.e. whether and to what extent Taylor's frozen eddies hypothesis, $u'_t \approx -\langle u_j \rangle u'_{x_j}$, holds.

In figure 9(a) we plot the spatial correlation coefficient between Eulerian acceleration u'_t and sum of streamwise mean and self-advection $u_j u'_{x_j} = \langle u_j \rangle u'_{x_j} + u'_j u'_{x_j}$, and in figure 9(b) their respective root mean square (rms) values. Large negative correlation coefficients, reaching nearly -1 at channel centre, between the Eulerian acceleration and streamwise advection across the channel indicate strong anti-correlating behaviour far enough from the wall. This cancellation behaviour is further consolidated by their similar rms values far enough from the wall, e.g. $y^+ \gtrsim 50$. In fact, the anti-correlation between the local Eulerian acceleration and the streamwise mean advection $\langle u \rangle u'_x$ is even stronger, as shown by the similar correlation coefficients in figure 9(c) and the rms peaks in figure 9(d), evidencing a large degree of applicability of Taylor's hypothesis where this anti-correlation is large enough. The spanwise mean advection is very small due to the small plane-average spanwise velocity $\langle w \rangle$, even in the current small computational domain. Removing the self-advection of fluctuating velocity field leads to stronger anti-correlation close to the wall. While the turbulent self-advection is relatively small compared to the mean advection, they still provide significant contribution to the overall shear-acceleration covariance, as shown by the magnitude of the covariance in figure 8(c) compared to that in figure 6(a).

It is noteworthy that Taylor's frozen eddies hypothesis appears valid with correlation coefficients between -0.85 and -1 in figure 9(c) at all distances from the wall, which confirms previous correlation analyses by Piomelli *et al.* (1989) and Geng *et al.* (2015). We can therefore conclude that the average convective nature of TCF testified by Taylor's hypothesis is largely responsible for the cancellation between the covariance of local fluctuating shear with fluctuating Eulerian acceleration (figure 8a) and the covariance of local fluctuating shear with mean advection (figure 8b) in this region. In the definition of the correlation coefficient (4.5), the plane-average mean velocity appearing in the numerator is factored out by itself in the denominator. The choice of such plane-average velocity plays no role in the value of the coefficient. The mean streamwise velocity $\langle u \rangle$ may in fact differ from the actual convection velocity, especially in the near-wall region, as detailed by Geng *et al.* (2015). As far as covariances of plane-fluctuating quantities are concerned, the choice of mean or convection velocity plays no role in the correlation analysis.

We have already noted that the shear-acceleration covariance in figure 6(a) provides the largest contribution to $\langle \tau'_w^2 \rangle$. It has a peak close to about $y^+ \approx 5$. Among the four covariances in figure 8, only the covariance between local fluctuating shear and the turbulence production-related term displays a peak below $y^+ < 10$ (figure 8d). It is this peak which is reflected in the shear-acceleration covariance peak seen in figure 6(a). These two peaks do not only share a similar y^+ location, they also display similar peak magnitudes, although the shear-acceleration covariance displays a Reynolds number dependence that is more pronounced than the shear-production covariance. We propose that it is the shear-production term that mainly determines the near-wall peak position of the shear-acceleration covariance in figure 6(a) and principally contributes to its peak magnitude, and that the other covariances in figure 8 contribute to the Reynolds number dependence.

4.4. Origin of the near-wall peak

In TCF, $\langle v \rangle(y, t) = 0$ at all y . Inside the x - z plane-average of shear-production covariance $-\langle u_y \rangle \langle u'_y v' \rangle$, one may consider the fluctuating local shear as a weight to the averaging of v' . For the weighted average $-\langle u'_y v' \rangle$ to be positive within the viscous sublayer, there must, for example, be an increased chance for u'_y to be large and positive wherever v' is negative, i.e. the two quantities must be dependent in their joint probability density function (JPDF) $P(v', u'_y)$. If they were independent from each other, we would have $P(v', u'_y) = P(v')P(u'_y)$ and then converting plane-averaging into expectations on the support of v' and u'_y :

$$-\langle v' u'_y \rangle = \int P(v', u'_y) d(v', u'_y) = \int P(v')P(u'_y) dv' du'_y = -\langle v' \rangle \langle u'_y \rangle = 0.$$

To demonstrate statistical dependence between two variables, we compare directly the joint PDF to the marginal PDFs in terms of point-wise mutual information (PMI) defined as:

$$\text{PMI}(v', u'_y) \equiv \ln \left(\frac{P(v', u'_y)}{P(v')P(u'_y)} \right) = \ln \left(\frac{P(v'|u'_y)}{P(v')} \right) = \ln \left(\frac{P(u'_y|v')}{P(u'_y)} \right) \quad (4.7)$$

Given a set of values (v', u'_y) , if the PMI is positive, $P(v', u'_y) > P(v')P(u'_y)$ and the probability density of the given values is greater than if the two variables were independent, hence they are statistically correlated. One may also interpret the PMI from a Bayesian point of view: the positive value of PMI indicates that the conditional probability of v' provided a value of u'_y is more probable than the marginal probability of v' without such condition and vice versa.

We plot in figure 10(a, c, e, g, i) the PMI of the fluctuating wall-normal velocity and the fluctuating streamwise shear around $y^+ \in [4, 5]$ where $-\langle u_y \rangle \langle v' u'_y \rangle$ reaches its maximum

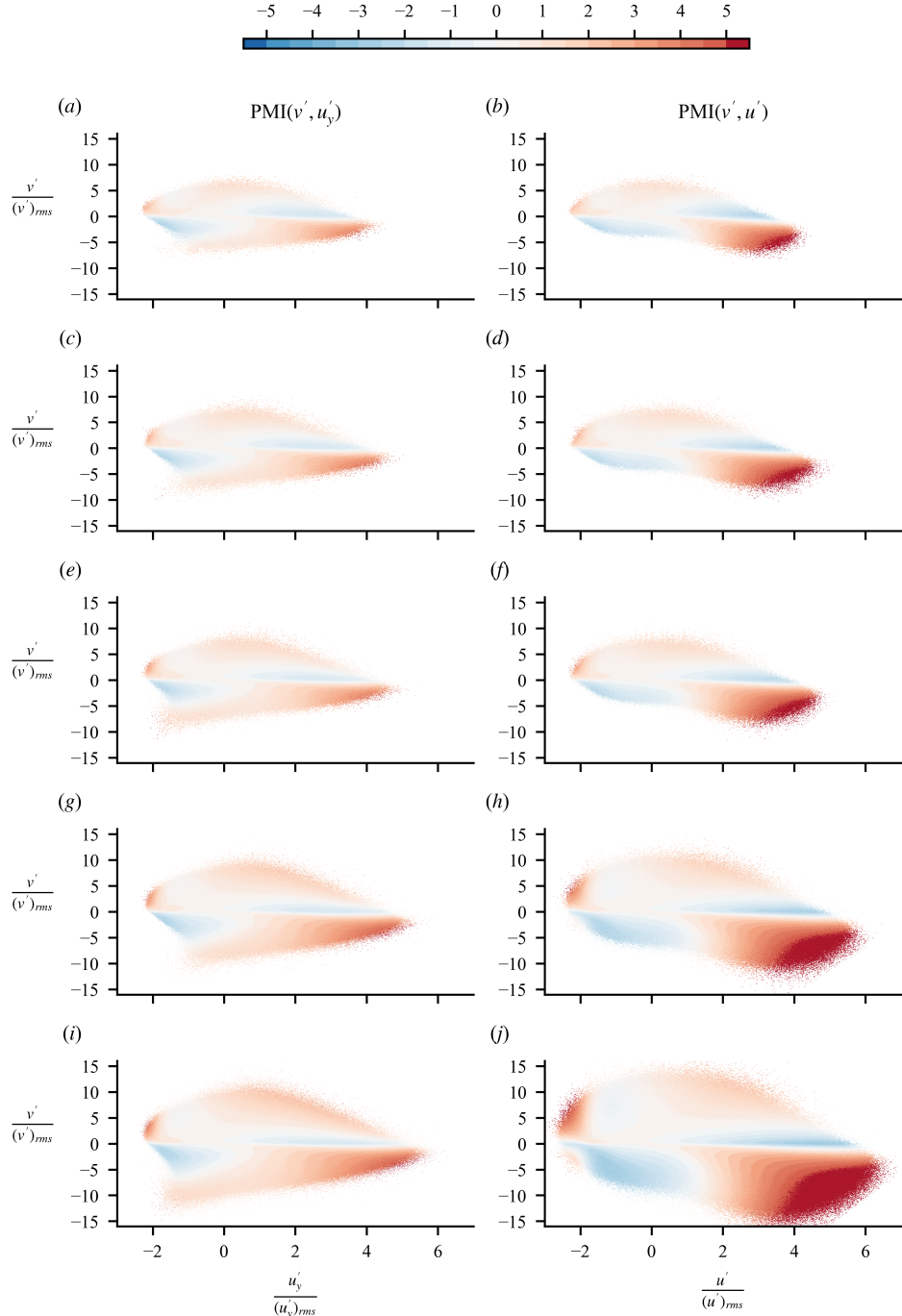


Figure 10: Point-wise mutual information at $y^+ \in [4, 5]$ where the shear-production covariance $-\overline{\langle u_y \rangle \langle v' u'_y \rangle}$ maximises. Left: (v', u'_y) ; right: (v', u') . (a, b) R230, (c, d) R360, (e, f) R500, (g, h) R950, (i, j) R2000. All quantities are normalised by their respective rms values.

in the viscous sublayer for five Reynolds numbers. A strong correlation with positive PMI is shown between the negative values of $v' < 0$ and large positive values of $u'_y > 0$, which contribute to the positive peak in $-\langle u_y \rangle \langle v' u'_y \rangle$. To further elucidate the origin of this local statistical dependence, we plot in figure 10(b, d, f, h, j) the pointwise mutual information for (v', u') at the same wall normal position. This time, the negative local v' is only significantly correlated with large positive u' (sweeps $u' > 0, v' < 0$) but not negative u' values. It is known that in wall-bounded turbulence ejections ($u' < 0, v' < 0$) and sweeps ($u' > 0, v' < 0$) make a dominant contribution to the Reynolds shear stress (see e.g. Pope 2000). Here we find that sweeps dominate the near-wall dynamics in the viscous sublayer with very high statistical dependence in terms of PMI between large positive u' and negative v' . In the viscous sublayer very near the wall, high values of u' imply high values of u'_y , hence the PMI of (v', u'_y) may be a consequence of the PMI of (v', u') at sweep events. Ejections also contribute to $-\langle u_y \rangle \langle v' u'_y \rangle$ and its sign but less significantly than sweeps as seen in both PMIs. Negative values of u' imply negative u'_y in the viscous sublayer very near the wall and so ejections contribute to the positive value $-\langle u_y \rangle \langle v' u'_y \rangle$ in the viscous sublayer. In conclusion, sweeps, predominantly, but also ejections dominate the shear-production covariance $-\langle u_y \rangle \langle v' u'_y \rangle$ around $y^+ \in [4, 5]$ in the viscous sublayer and, in turn, the near-wall peak of the shear-acceleration covariance in figure 6(a).

Sweeps typically originate far away from the wall so that their size and strength should be, at least partially, characterised by outer units at sufficiently high Reynolds number. They can therefore impose some outer flow and Reynolds number dependence on the shear-acceleration covariance and, as a result, on the variance of the fluctuating wall shear stress. Furthermore, with increasing Reynolds number, it is observed that the support of u_y expands in figure 10(a, c, e, g, i), favouring increasing extreme events in the near-wall region. As the fluctuating velocities and their gradients become more intermittent and more extreme, the higher order statistics will also start to show differences with increasing Reynolds number. We observe that the second-order statistical quantity $-\langle u_y \rangle \langle v' u'_y \rangle$ is very weakly dependent on Reynolds number below $y^+ < 10$ for our range of Reynolds numbers. On the contrary, the shear-self-advection covariance $-\langle u'_y (u'_j u'_{x_j}) \rangle$ as a third-order statistical quantity shows stronger variation with Reynolds number, which might be explained by increased intermittency in the region not very far from the wall (e.g. $y^+ \approx 10$).

5. Conclusion

We have studied the relation between the wall shear stress and the fluid flow above the wall in a fully developed turbulent channel flow (FD TCF). Without any preconception (concerning, for example, energy or momentum balance), the Navier-Stokes equations naturally imply that the mean wall shear stress can be obtained from mean streamwise shear and mean streamwise acceleration in the flow, and that the variance of the fluctuating wall shear stress can be obtained from correlations between fluctuating streamwise shear and fluctuating streamwise acceleration predominantly as well as correlations between fluctuating streamwise shear and fluctuating pressure gradient in the flow. At the Reynolds numbers accessible by our FD TCF DNS data, it is enough to integrate these flow statistics from the wall to the outer edge of the buffer layer, see equations (3.5) and (4.4). In other words, information within the buffer layer is sufficient to determine the mean wall shear stress and the variance of the fluctuating wall shear stress to very good accuracy, at least at the Reynolds numbers considered here. Above the buffer layer, the fluctuating streamwise acceleration near-balances the fluctuating pressure gradient so that the correlations between fluctuating streamwise shear

and fluctuating streamwise acceleration and the correlations between fluctuating streamwise shear and fluctuating pressure gradient effectively cancel each other. The outer bound δ_w in the integrals in these two equations appears to scale with the wall unit δ_v , but very weak dependencies of δ_w on Re_τ are conceivable in equations (3.5) and (4.4). In fact there may be two different δ_w scales defined by slightly different Reynolds number dependencies, a weaker one for (3.5) and a slightly stronger one for in (4.4). Our data do not reach high enough values of Re_τ to determine these Re_τ dependencies.

Even though equations (3.5) and (4.4) imply that one can find between the wall and the outer edge of the buffer layer all the flow information required for a good estimation of the mean wall shear stress and the variance of the wall shear stress fluctuations, this does not mean that the wall shear stress statistics do not depend on the outer flow. The mean streamwise acceleration, the correlation between fluctuating streamwise shear and fluctuating streamwise acceleration and the correlation between fluctuating streamwise shear and fluctuating pressure gradient between the wall and the buffer layer have Reynolds number dependencies which betray a dependence on the outer flow.

Some understanding of the correlations between fluctuating streamwise shear and fluctuating streamwise acceleration which dominate the variance of the fluctuating wall shear stress has been obtained by using a Reynolds decomposition of the streamwise velocity to decompose the fluctuating streamwise acceleration into four terms plus a plane-average term (see equation 4.6). This approach reveals cancellations caused by Taylor's frozen eddies hypothesis which proves to be a good approximation at all distances from the wall.

Finally, it is the turbulence production-related term in the decomposition (4.6) of the fluctuating streamwise acceleration which accounts for the near-wall peak of the shear-acceleration covariance in the viscous sub-layer. Sweeps, and to a lesser extent, ejections dominate the shear-production covariance $-\langle u_y' \rangle \langle v' u_y' \rangle$ around $y^+ \in [4, 5]$ and, in turn, the near-wall peak of the shear-acceleration covariance in the viscous sub-layer.

Funding. This work is supported by the European Office of Aerospace Research and Development (EOARD) (FA8655-21-1-7016; Program Manager: Dr D. Smith).

Acknowledgements. This work is granted access to the HPC resources of IDRIS under the allocation 2022-021741 made by GENCI (Grand Equipement National de Calcul Intensif) and Zeus supercomputers (Mésocentre de Calcul Scientifique Intensif de l'Université de Lille)

Declaration of interests. The authors report no conflict of interest.

Appendix A. Derivation of n th order wall shear stress equation

The plane-fluctuating streamwise Navier-Stokes equation is:

$$a'_u = -p'_x + \nu u'_{//} + \nu u'_{yy}. \quad (\text{A } 1)$$

We multiply the fluctuating equation with $n(vu'_y)^{n-1}$ at the same (x, y, z) for some integer $n > 1$, the wall-normal diffusion term (due to product rule) becomes:

$$n(vu'_y)^{n-1} \nu u'_{yy} = \frac{\partial}{\partial y} (vu'_y)^n. \quad (\text{A } 2)$$

Averaging the premultiplied fluctuating streamwise Navier-Stokes equation in x - z plane and integrating from the wall up to some arbitrary y :

$$\begin{aligned}
\int_0^y \langle n(vu'_y)^{n-1} a'_u \rangle dy &= - \int_0^y \langle n(vu'_y)^{n-1} p'_x \rangle dy \\
&\quad + \int_0^y \langle n(vu'_y)^{n-1} vu'_{//} \rangle dy + \int_0^y \langle n(vu'_y)^{n-1} vu'_{yy} \rangle dy \\
&\Downarrow \text{using (A 2)} \\
\int_0^y \langle n(vu'_y)^{n-1} a'_u \rangle dy &= - \int_0^y \langle n(vu'_y)^{n-1} p'_x \rangle dy \\
&\quad + \int_0^y \langle n(vu'_y)^{n-1} vu'_{//} \rangle dy + \langle (vu'_y)^n \rangle(y) - \langle (vu'_y)^n \rangle(y=0)
\end{aligned}$$

Rearranging, we obtain an equation for n th order wall shear stress:

$$\begin{aligned}
\langle \tau'_w^n \rangle &= -n\nu^{n-1} \int_0^y \langle u'_y^{n-1} a'_u \rangle dy \\
&\quad - n\nu^{n-1} \int_0^y \langle u'_y^{n-1} p'_x \rangle dy \\
&\quad + n\nu^n \int_0^y \langle u'_y^{n-1} u'_{//} \rangle dy \\
&\quad + \langle (vu'_y)^n \rangle(y)
\end{aligned} \tag{A 3}$$

REFERENCES

AFZAL, N. 1984 Mesolayer theory for turbulent flows. *AIAA Journal* **22** (3), 437–439.

AGOSTINI, L. & LESCHZINER, M. 2019 The connection between the spectrum of turbulent scales and the skin-friction statistics in channel flow at $Re_\tau \approx 1000$. *Journal of Fluid Mechanics* **871**, 22–51.

ALFREDSSON, P. H., JOHANSSON, A. V., HARITONIDIS, J. H. & ECKELMANN, H. 1988 The fluctuating wall-shear stress and the velocity field in the viscous sublayer. *The Physics of Fluids* **31** (5), 1026–1033.

BEWLEY, T. 2014 *Numerical Renaissance: Simulation, Optimization, and Control*. Renaissance Press.

DIAZ-DANIEL, C., LAIZET, S. & VASSILICOS, J. C. 2017 Wall shear stress fluctuations: Mixed scaling and their effects on velocity fluctuations in a turbulent boundary layer. *Physics of Fluids* **29** (5), 055102.

ELNAHHAS, A. & JOHNSON, P. L. 2022 On the enhancement of boundary layer skin friction by turbulence: an angular momentum approach. *Journal of Fluid Mechanics* **940**, A36.

FUKAGATA, K., IWAMOTO, K. & KASAGI, N. 2002 Contribution of reynolds stress distribution to the skin friction in wall-bounded flows. *Physics of Fluids* **14** (11), L73–L76.

GENG, C.-H., HE, G.-W., WANG, Y.-S., XU, C.-X., LOZANO-DURÁN, A. & WALLACE, J. M. 2015 Taylor's hypothesis in turbulent channel flow considered using a transport equation analysis. *Physics of Fluids* **27** (2), 025111.

HWANG, Y. & BENGANA, Y. 2016 Self-sustaining process of minimal attached eddies in turbulent channel flow. *J. Fluid Mech.* **795**, 708–738.

HWANG, Y. & COSSU, C. 2010 Self-sustained process at large scales in turbulent channel flow. *Phys. Rev. Lett.* **105**, 044505.

HWANG, Y. & LEE, M. 2020 The mean logarithm emerges with self-similar energy balance. *J. Fluid Mech.* **903**, R6.

KIM, J. & MOIN, P. 1985 Application of a fractional-step method to incompressible Navier-Stokes equations. *J. Comp. Phys.* **59** (2), 308–323.

KLINNER, J. & WILLERT, C. E. 2025 Measurements of the unsteady wall shear stress vector using multi-aperture defocusing microscopic particle tracking velocimetry. *Experimental Thermal and Fluid Science* **163**, 111395.

VON KÁRMÁN, TH. 1921 Über laminare und turbulente reibung. *Z. Angew. Math. Mech.* **1** (4), 233–252.

LEE, M. & HWANG, Y. 2025 Turbulent transport for wall-shear-stress fluctuations. *Journal of Fluid Mechanics* **1023**, A48.

LEE, M. & MOSER, R. D. 2015 Direct numerical simulation of turbulent channel flow up to $Re_\tau \approx 5200$. *J. Fluid Mech.* **774**, 395–415.

LIGRANI, P. M. & MOFFAT, R. J. 1986 Structure of transitionally rough and fully rough turbulent boundary layers. *Journal of Fluid Mechanics* **162**, 69–98.

LOZANO-DURÁN, A. & JIMÉNEZ, J. 2014 Effect of the computational domain on direct simulations of turbulent channels up to $Re_\tau = 4200$. *Phys. Fluids* **26** (1), 011702.

PANTON, R. L. 2007 Composite asymptotic expansions and scaling wall turbulence. *Phil. Trans. R. Soc. A* **365** (1852), 733–754.

PIOMELLI, U., BALINT, J.-L. & WALLACE, J. M. 1989 On the validity of Taylor's hypothesis for wall-bounded flows. *Physics of Fluids A: Fluid Dynamics* **1** (3), 609–611.

POPE, S. B. 2000 *Turbulent Flows*. Cambridge University Press.

RAVIKUMAR, K., SUBBIAH, R., RANGANATHAN, N., BENSINGH, J., KADER, A. & NAYAK, S.K. 2020 A review on fatigue damages in the wind turbines: Challenges in determining and reducing fatigue failures in wind turbine blades. *Wind Engineering* **44** (4), pp. 434–451.

RENARD, N. & DECK, S. 2016 A theoretical decomposition of mean skin friction generation into physical phenomena across the boundary layer. *Journal of Fluid Mechanics* **790**, 339–367.

RICCO, P. & SKOTE, M. 2022 Integral relations for the skin-friction coefficient of canonical flows. *Journal of Fluid Mechanics* **943**, A50.

SCHLATTER, P. & ÖRLÜ, R. 2010 Assessment of direct numerical simulation data of turbulent boundary layers. *Journal of Fluid Mechanics* **659**, 116–126.

TSINOBER, A., VEDULA, P. & YEUNG, P. K. 2001 Random taylor hypothesis and the behavior of local and convective accelerations in isotropic turbulence. *Physics of Fluids* **13** (7), 1974–1984.

WILLERT, C.E., CUVIER, C., FOUCAUT, J.M., KLINNER, J., STANISLAS, M., LAVAL, J.P., SRINATH, S., SORIA, J., AMILI, O., ATKINSON, C., KÄHLER, C.J., SCHARNOWSKI, S., HAIN, R., SCHRÖDER, A., GEISLER, R., AGOCS, J. & RÖSE, A. 2018 Experimental evidence of near-wall reverse flow events in a zero pressure gradient turbulent boundary layer. *Experimental Thermal and Fluid Science* **91**, 320–328.

XIA, Q.-J., HUANG, W.-X., XU, C.-X. & CUI, G.-X. 2015 Direct numerical simulation of spatially developing turbulent boundary layers with opposition control. *Fluid Dyn. Res.* **47** (025503).

YEO, K., KIM, B.-G. & LEE, C. 2010 On the near-wall characteristics of acceleration in turbulence. *Journal of Fluid Mechanics* **659**, 405–419.

YIN, L., HWANG, Y. & VASSILICOS, J. C. 2024 Dynamics of turbulent energy and dissipation in channel flow. *Journal of Fluid Mechanics* **996**, A12.

YOON, M., AHN, J., HWANG, J. & SUNG, H.J. 2016 Contribution of velocity-vorticity correlations to the frictional drag in wall-bounded turbulent flows. *Physics of Fluids* **28** (8), 081702.

ZHAO, Y., FAN, Y. & LI, W. 2024 Reynolds number effects on a velocity–vorticity correlation-based skin-friction drag decomposition in incompressible turbulent channel flows. *Journal of Fluid Mechanics* **979**, A20.

ZHOU, M.L., YU, Y.F., CHEN, R.Y., LIU, X.C., HU, Y.L., MA, Z.Y., GAO, L.W., JIAN, W.X. & WANG, L.P. 2023 Wall shear stress and its role in atherosclerosis. *Frontiers in Cardiovascular Medicine* **10**.

ÖRLÜ, R. & VINUESA, R. 2020 Instantaneous wall-shear-stress measurements: advances and application to near-wall extreme events. *Measurement Science and Technology* **31** (11), 112001.